

Magnetic properties of geometrically frustrated SrGd_2O_4

O. Young,¹ G. Balakrishnan,¹ M. R. Lees,¹ and O. A. Petrenko¹

¹*Department of Physics, University of Warwick, Coventry CV4 7AL, United Kingdom*

(Dated: August 13, 2014)

A study of the magnetic properties of the frustrated rare earth oxide SrGd_2O_4 has been completed using bulk property measurements of magnetization, susceptibility and specific heat on single crystal samples. Two zero-field phase transitions have been identified at 2.73 and 0.48 K. For the field, H , applied along the a and b axes, a single boundary is identified that delineates the transition from a low field, low temperature magnetically ordered regime to a high field, high temperature paramagnetic phase. Several field-induced transitions, however, have been observed with $H \parallel c$. The measurements have been used to map out the magnetic phase diagram of SrGd_2O_4 , suggesting that it is a complex system with several competing magnetic interactions. The low-temperature magnetic behavior of SrGd_2O_4 is very different compared to the other SrLn_2O_4 (Ln = Lanthanide) compounds, even though all of the SrLn_2O_4 compounds are isostructural, with the magnetic ions forming a low-dimensional lattice of zigzag chains that run along the c axis. The differences are likely to be due to the fact that in the ground state Gd^{3+} has zero orbital angular momentum and therefore the spin-orbit interactions, which are crucial for other SrLn_2O_4 compounds, can largely be neglected. Instead, given the relatively short $\text{Gd}^{3+}\text{-Gd}^{3+}$ distances in SrGd_2O_4 , dipolar interactions must be taken into account for this antiferromagnet alongside the Heisenberg exchange terms.

PACS numbers: 75.47.Lx, 75.50.Ee, 75.30.Cr, 75.30.Gw, 75.40.-s

I. INTRODUCTION

Geometrical frustration arises in systems where the interactions between the magnetic moments are incompatible with their spatial arrangement in a lattice, so that at low temperatures not all of the interaction energies can be simultaneously minimized.¹⁻³ Thus, in the presence of antiferromagnetic exchange interactions, many magnets based on corner- or edge-sharing triangles⁴⁻⁶ or tetrahedra⁷⁻⁹ can exhibit geometric frustration. A general consequence of frustration is the establishment of magnetic order at temperatures much lower than what would be expected from the strength of the exchange interactions, and the absence of magnetic order down to the lowest measured temperatures.¹⁰⁻¹³ While some frustrated systems remain in a highly degenerate manifold of ground states, others form a unique ground state at very low temperatures. In this regime small perturbations to the Hamiltonian, such as further-neighbour exchange, single-ion anisotropy, magnetic dipolar interactions, etc., as well as other effects such as quantum fluctuations, become important and can lead to unusual spin arrangements. New geometrically frustrated systems are constantly being discovered, and their behavior is often complex, with a rich variety of low-temperature properties.

The SrLn_2O_4 (Ln = Lanthanide) family of compounds,¹⁴ which crystallise in the form of calcium ferrite,¹⁵ space group $Pn\bar{m}$, have been suggested as lattices that could give rise to frustrated magnetism. For the case of SrGd_2O_4 , the magnetic Gd^{3+} ions are linked in a network of triangles and hexagons, as shown in Fig. 1, and there are two crystallographically inequivalent sites for the rare earth ions (which are shown in red and blue). Along the c axis, the magnetic ions form zigzag chains and the nearest distance between the Gd^{3+} ions is about

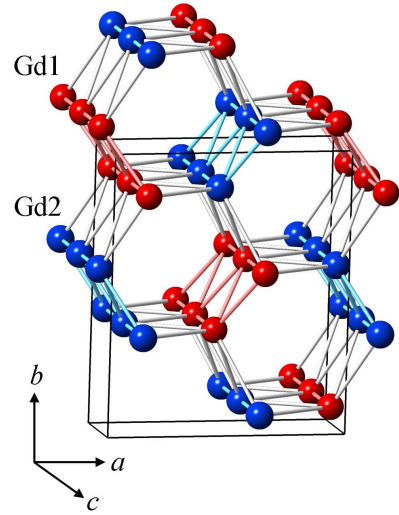


FIG. 1: Positions of the magnetic ions in SrGd_2O_4 , with the two crystallographically inequivalent sites of the rare earth ions shown in different colors (red and blue). When viewed in the a - b plane, honeycombs of the Gd^{3+} ions are visible. Zigzag chains running along the c axis connect the honeycomb layers and give rise to geometric frustration. The box indicates the dimensions of the crystallographic unit cell.

3.48 Å.¹⁶ The zigzag chains (shown with either red or blue bonds) which consist of the Gd^{3+} ions sitting in the same crystallographic positions have shorter $\text{Gd}^{3+}\text{-Gd}^{3+}$ separations across the zigzags (3.54 to 3.62 Å) as compared to the longer bonds (shown in gray, 3.85 to 4.12 Å), which connect the Gd^{3+} ions at inequivalent positions.¹⁶ The zigzag structures can be frustrated if the dominant exchange is antiferromagnetic, and are magnetically equivalent to spin chains with first- and second-

nearest-neighbor interactions. The chains of Gd^{3+} ions interconnect by forming a distorted *honeycomb* structure, a bipartite lattice made up of edge sharing hexagons, in the a - b plane.

The magnetic characterization of powder samples of the SrLn_2O_4 family of compounds began with the work of Karunadasa *et al.*¹⁷ In this early study, measurements of the magnetic susceptibility for all of the SrLn_2O_4 compounds had revealed a disparity in the measured Weiss temperatures, θ_{CW} , and the lack of long-range order down to 1.8 K.¹⁷ Single crystals of these oxides have been grown,^{18,19} and four members of the SrLn_2O_4 family, where $\text{Ln} = \text{Dy}$,²⁰ Ho ,²¹⁻²⁵ Er ,^{21,26} and Yb ,¹⁹ have been studied in detail. Despite the large reported values of the Weiss temperatures (-13.5 to -99.4 K),¹⁷ measurements of the low-temperature susceptibility and heat capacity on the SrHo_2O_4 ,²¹ SrEr_2O_4 ,²⁶ and SrYb_2O_4 ¹⁹ materials revealed that their ordering temperatures are all below 1 K, and for SrDy_2O_4 ²⁰ no transitions to long-range order have been observed. All the compounds also show signs of short-range correlations in the bulk properties. This short-range order has been further investigated using neutron diffraction measurements, and these have revealed a rich variety of low-temperature, low-dimensional magnetic behavior.^{19,22,26-28} The application of a magnetic field induces a variety of transitions in all of the SrLn_2O_4 compounds.²⁸ The crystals are highly anisotropic, and for SrEr_2O_4 , and SrHo_2O_4 and SrDy_2O_4 plateaux in the magnetization curves at approximately one third of the saturation value, appear for certain values of the applied field. Such features are usually indicative of the stabilization of a collinear two-spins-up one-spin-down (uud) structure.

In this paper, we report on the low-temperature properties of SrGd_2O_4 , single crystals of which have been grown for the first time using the floating zone technique and examined using susceptibility, $\chi(T)$, magnetization, $M(H)$, and specific heat, $C(T)$ and $C(H)$, measurements. The magnetic Gd^{3+} ions have rather different electronic properties compared to the other lanthanides (as they are almost isotropic in the ground state where the orbital angular momentum is zero), and hence the magnetic behavior of SrGd_2O_4 is expected to be markedly different to the other members of the SrLn_2O_4 series. Our preliminary measurements of $\chi(T)$ and $M(H)$ on a powder sample of SrGd_2O_4 , indicated that there *are* transitions in this compound at 2.73 K in $\chi(T)$ and around 19 kOe in $M(H)$, contrary to what has been reported in Ref. 17. These transitions were probably missed in the previous investigation as a result of having too large a step size in field, H , and temperature, T , during the data collection. Low-temperature measurements of $\chi(T)$ on single crystal samples for the fields applied along each of the principal axes, show that below 2.73 K the most dramatic changes in the susceptibility occur when the field is applied along the c axis. Low-temperature $M(H)$ data indicate that the magnetization processes along the a and b axes are quite uneventful,

Atom	x	y
Sr	0.7506(5)	0.6489(4)
Gd1	0.4270(4)	0.1127(3)
Gd2	0.4161(4)	0.6110(3)
O1	0.220(3)	0.181(2)
O2	0.135(3)	0.479(3)
O3	0.510(3)	0.785(2)
O4	0.423(4)	0.420(2)

TABLE I: Refined crystal structure parameters for SrGd_2O_4 at room temperature. All the atoms occupy the $4c$ ($x, y, 0.25$) site of the space group $Pnam$ with the lattice parameters $a = 10.1321(1)$, $b = 12.0614(1)$ and $c = 3.47566(2)$ Å.

but that there are several in-field transitions when H is applied along the c axis. For $H \parallel a$ and $H \parallel b$ a single boundary is identified that delineates the transition from a low field, low temperature magnetically ordered regime to a high field, high temperature paramagnetic phase. Specific heat measurements on the single crystals of SrGd_2O_4 were first performed in zero field, and these indicate that in addition to the transition seen at 2.73 K, another transition at an even lower temperature of 0.48 K is observed. $C(T)$ in several applied fields and $C(H)$ at a range of temperatures were also measured, and the results of all the bulk property measurements have been used to construct an H - T phase diagram of SrGd_2O_4 . Multiple magnetic phases have been identified, and this suggests that the magnetic ordering scheme in SrGd_2O_4 is quite complex and rather different to that of the other SrLn_2O_4 compounds. This is likely to be due to the fact that in the ground state the Gd^{3+} ions have zero orbital angular momentum. Hence, crystal-field splittings are expected to be less important in SrGd_2O_4 , making it the best candidate in the SrLn_2O_4 series for a realisation of a classical Heisenberg exchange antiferromagnet. Dipole-dipole interactions are expected to be the leading perturbations in the Hamiltonian. SrGd_2O_4 thus provides an interesting comparison and furthers the study of the influence of the spin-spin and spin-orbit interaction on the physics of the SrLn_2O_4 ²⁹ and similar systems, such as BaLn_2O_4 .³⁰⁻³²

II. EXPERIMENTAL DETAILS

Single crystal samples of SrGd_2O_4 were grown using the floating zone method, similar to the procedure reported in Ref. 18. Initially, powder SrGd_2O_4 samples were prepared from high purity (99.99%) starting compounds SrCO_3 and Gd_2O_3 , in an off-stoichiometric ratio of 1 : 0.875 (as it was found from x-ray diffraction measurements that when powders were mixed in a stoichiometric ratio the final materials contained a large, $\sim 15\%$, impurity phase of Gd_2O_3). Following the proce-

ture described for the earlier syntheses of SrGd_2O_4 ,^{14,17} the powders were ground together and fired at ambient pressure in air at 1350°C for a total of 48 hours in an alumina crucible. In general, one intermediate grinding was used to ensure homogeneity of the mixtures. The purity of the SrGd_2O_4 powder was verified by performing a Rietveld refinement³³ using x-ray diffraction data collected at room temperature, and allowing for two phases in the material - the desired SrGd_2O_4 and an impurity phase of the starting compound Gd_2O_3 . The results suggest that the SrGd_2O_4 sample that was prepared starting with an off-stoichiometric $\text{SrCO}_3/\text{Gd}_2\text{O}_3$ ratio is 99.80% pure SrGd_2O_4 , with $\chi^2 = 1.158$ obtained for the fit. The atomic positions for SrGd_2O_4 (within the orthorhombic space group $Pnam$) are given in Table I together with the refined unit cell parameters.

The SrGd_2O_4 powder was subsequently isostatically pressed into rods of ~ 7 mm diameter and ~ 80 mm in length, and sintered in air at 1100°C for 24 hours. Since no previous SrGd_2O_4 crystals existed, to start the growth, a polycrystalline rod was used as a “seed”. A high temperature optical furnace (Crystal Systems Inc. Optical Floating Zone Furnace Model FZT-12000-X-VI-VP) equipped with four Xe arc lamps focused by four ellipsoidal mirrors was used. The feed and seed rods were counter-rotated at 10-20 rpm, and growth speeds ranging from 3 to 6 mm h^{-1} were used. Several atmospheres were tried for the growth of SrGd_2O_4 , but the best results were obtained for growths carried out in air at ambient pressure. The SrGd_2O_4 crystals grown in this manner were transparent to light, but were not wholly crack free, although large single crystal regions could be isolated.

Once the crystal was produced, several samples were aligned using a backscattering x-ray Laue method and cut into thin rectangular prisms with faces perpendicular to the principal crystal axes. The samples varied from 10 to 15 mg for magnetization and magnetic susceptibility to 0.14 to 12.5 mg for specific heat measurements. Demagnetization corrections were applied following Aharoni.³⁴

A Quantum Design SQUID magnetometer was used to measure the magnetic susceptibility and magnetization along each of the principal crystallographic directions (with the applied field within an estimated 3° accuracy of the principal axes) in the ranges of $0.5 < T < 400$ K and $0 < H < 70$ kOe. The temperature range was extended below 1.8 K using an iQuantum [IQ2000- AGHS-2RSO ^3He system] refrigerator insert.³⁵ Additional higher-field (up to 100 kOe) magnetization measurements were performed using an Oxford Instruments vibrating sample magnetometer (VSM) with the lowest achievable temperature of 1.4 K.

Specific heat measurements were performed using a Quantum Design calorimeter, with the addition of a ^3He insert, and were carried out both in zero field in the temperature range of $0.4 < T < 400$ K, and for the fields of up to 90 kOe applied along the c axis. The heat capacity of single crystal samples of SrY_2O_4 and SrLu_2O_4 , which are non-magnetic and isostructural to SrGd_2O_4 ,

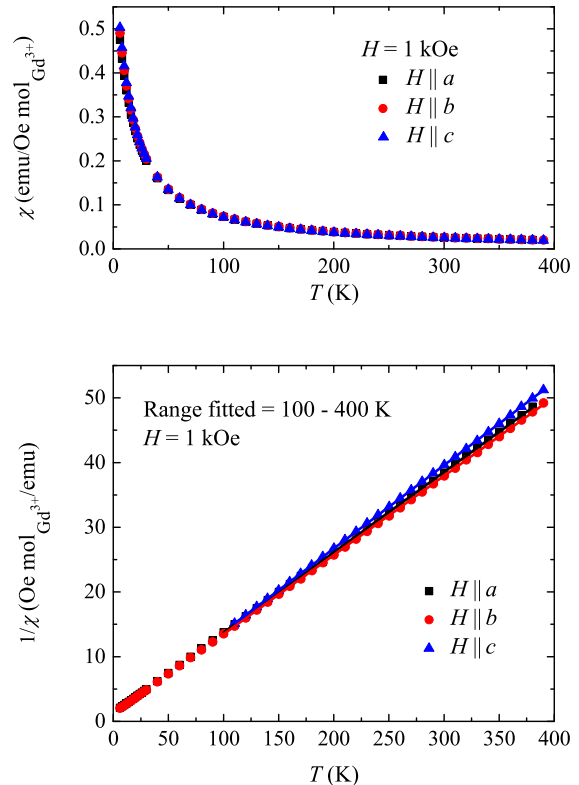


FIG. 2: Top: Magnetic susceptibility versus temperature in an applied field of 1 kOe in the temperature range of 6 to 400 K for the field applied along the three principal axes of a single crystal sample of SrGd_2O_4 . Bottom: Reciprocal of the molar susceptibility versus temperature and the least-squares regression fits to the data (using the Curie-Weiss model).

allowed for an estimation of the lattice contribution to the specific heat.

III. RESULTS AND DISCUSSION

A. Temperature dependence of the magnetic susceptibility

1. High-temperature limit

The top panel of Fig. 2 shows the magnetic susceptibility versus temperature in 1 kOe, for a field applied along each of the three principal axes for a single crystal sample of SrGd_2O_4 . The bottom panel of Fig. 2 presents the temperature dependence of the inverse susceptibility. Here, the data are fitted to straight lines in the temperature range of 100 to 400 K. The parameters of these fits, the Weiss temperatures, θ_{CW} , and the calculated effective moments per magnetic ion, μ_{eff} , are listed in Table II. The average value of μ_{eff} is relatively close to the theoretical limit of $7.94 \mu_{\text{B}}$, predicted for the free ion

	$H \parallel a$	$H \parallel b$	$H \parallel c$	Mean	Powder
$\mu_{\text{eff}} (\mu_B)$	8.03(8)	8.10(5)	7.88(2)	8.00(3)	8.03(1)
$\theta_{\text{CW}} (\text{K})$	-11.0(6)	-7.4(2)	-12.3(1)	-10.3(2)	-10.4(1)

TABLE II: μ_{eff} and θ_{CW} for the fits of the data collected with the field applied along each of the principal axes of a single crystal sample of SrGd_2O_4 , their average values and a comparison to the data collected for a powder sample of SrGd_2O_4 . The value of the effective moment is close to $7.94 \mu_B$,³⁶ which is calculated using Hund's rules for a Gd^{3+} ion.

using Hund's rules. The average value of θ_{CW} is consistent with $\theta_{\text{CW}} = -10.4(1) \text{ K}$, which is obtained from our measurements made on a powder sample of SrGd_2O_4 , and this is comparable to the value of $-9.0(6) \text{ K}$ obtained by Karunadasa, *et al.*¹⁷

There are *no* large differences in the Weiss temperatures or the effective moments for the three principal crystal directions of SrGd_2O_4 , contrary to what is observed for the other SrLn_2O_4 compounds.^{19,21} It is likely that for all the SrLn_2O_4 compounds other than SrGd_2O_4 , the differences in the high-temperature susceptibility curves are due to the effects of low-lying crystal field levels.²⁴ For SrGd_2O_4 , however, in the ground state Gadolinium has a pure spin magnetic moment, and thus there is no distortion of the spherical $4f$ charge density due to the spin-orbit coupling, and hence no corresponding crystal field anisotropy.

2. Low-temperature limit

The low-temperature susceptibility measurements on the single crystal samples of SrGd_2O_4 are presented in Fig. 3 for a field of 100 Oe applied along the a , b , and c directions. Here, a small cusp in the susceptibility at 2.73 K for the a and b axes, and a large decrease $\chi(T)$ when the field is applied along the c axis suggests the presence of a phase transition, with the region of interest highlighted in the inset to Fig. 3. This is the first indication of a transition to a long-range ordered state identified for this compound, and the phase transition temperature appears to be much higher than that recorded for the other members of the SrLn_2O_4 series of compounds. Around the transition temperature, in low applied fields such as 100 Oe, there is only a slight difference between the data obtained on warming after cooling in field (FC) and the zero-field-cooled warming (ZFC) regimes, which suggests that the magnetic susceptibility of SrGd_2O_4 is not particularly sensitive to sample history.

The lowest reachable experimental temperature when measuring magnetic susceptibility with the aid of a ^3He probe is $\sim 0.5 \text{ K}$. Unfortunately this is not low enough to observe the second transition seen at 0.48 K in zero field for a powder sample of SrGd_2O_4 using heat capacity (see Section III C). However, the susceptibility data, acquired

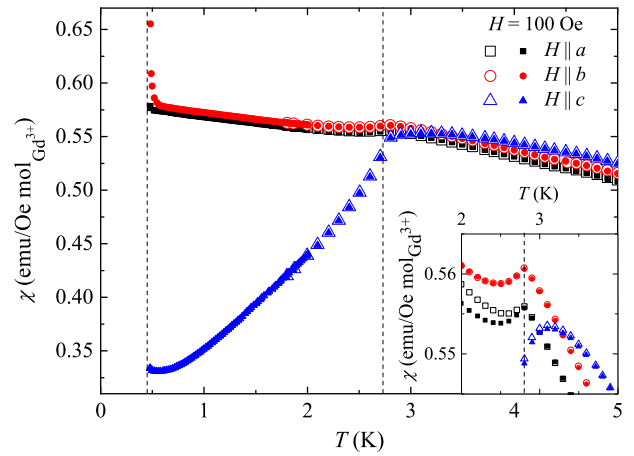


FIG. 3: Magnetic susceptibility obtained in the temperature range of 0.5 to 5 K for a field 100 Oe applied along each of the three principal axes of SrGd_2O_4 . Two dashed lines represent 0.48 K and 2.73 K, where λ -anomalies were observed in heat capacity data in zero field. A cusp is seen in the susceptibility at 2.73 K when the field is applied along either the a or b axes, while a sharp decrease occurs in $\chi(T)$ for a field applied along the c axis, which is highlighted in the inset. Also, below 2.73 K, small differences between ZFC (closed symbols) and FC (open symbols) measurements become apparent for $H \parallel a$.

at low fields (such as 0.1 kOe in Fig. 3), along all of the principal axes of SrGd_2O_4 show an upturn in $\chi(T)$ at the lowest temperatures, hinting to the presence of a second transition in SrGd_2O_4 at temperatures just below 0.5 K.

The temperature dependences of the magnetic susceptibilities in a range of fields applied along the a and b axes of SrGd_2O_4 are shown in the top panels of Fig. 4. No extra features are observed in larger fields. The low-temperature magnetic susceptibility curves obtained in the temperature range of 0.5 to 5 K, and field range of 0.1 to 50 kOe, with the fields applied along the c axis of SrGd_2O_4 are shown in the bottom panel of Fig. 4. Upon the application of field, the transition seen at 2.73 K is suppressed to lower temperatures. In fields between 20 and 30 kOe a second feature in the magnetic susceptibility is observed, and in fields above 30 kOe, only a single cusp in the low-temperature susceptibility is visible. This suggests a rich $H - T$ phase diagram for the fields applied along this axis of SrGd_2O_4 , and this will be discussed in Section III D.

B. Field dependence of the magnetization

The field dependence of the magnetization and its derivative obtained with the field applied along the principal axes of SrGd_2O_4 at 0.5 K are shown in Fig. 5. In lower fields, the data collected for $H \parallel a$ shows no features in dM/dH which remains small and practically flat. A similar behavior is observed for $H \parallel b$. In higher fields, both for $H \parallel a$ and $H \parallel b$, the magnetization deviates

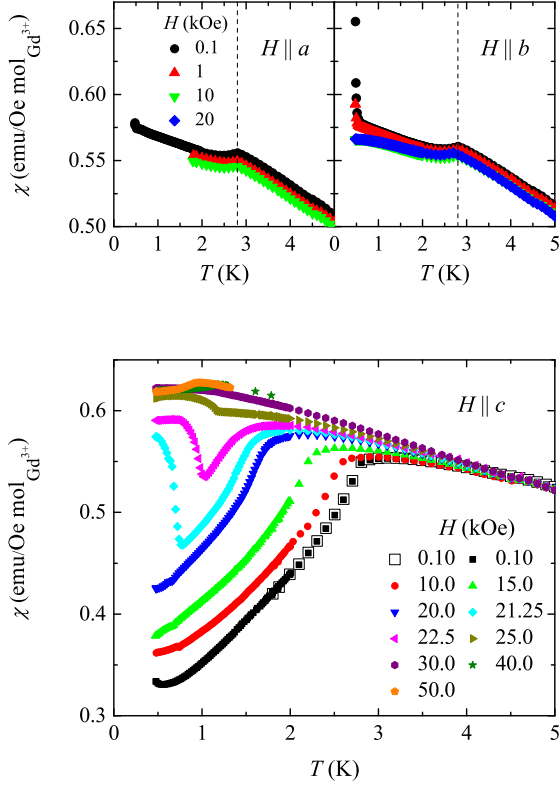


FIG. 4: Top: Temperature dependence of the magnetic susceptibility in different fields applied along the (left) a and (right) b axes of SrGd_2O_4 . There seems to be very little difference in the behavior at low fields and upon increasing the applied field along these axes. Bottom: low-temperature magnetic susceptibility obtained in the temperature range of 0.5 to 5 K, and field range of 0.10 to 50 kOe, with the fields applied along the c axis of SrGd_2O_4 . The transition seen at 2.73 K is suppressed by the application of higher fields, and in fields between 20 and 30 kOe a second feature in the magnetic susceptibility is observed. In fields above 30 kOe, again, only a single cusp in the low-temperature susceptibility is visible.

from a nearly straight line and shows signs of tending towards saturation, but being limited to a maximum field of 70 kOe (which after taking into account demagnetizing effects becomes even lower) it is difficult to accurately define the critical fields, therefore the error bars for the critical fields are relatively large. However, we have been able to clearly observe the magnetic saturation transitions for the field applied along either a or b axes of SrGd_2O_4 at temperatures above 1.4 K taking advantage of the higher fields available in the VSM (data not shown). Upon raising the temperature, the saturation transition moves gradually to lower fields and disappears completely above 2.73 K. The $M(H)$ and $M(T)$ data collected using the VSM for fields applied along either the a or b axes are combined with the SQUID data to construct the phase diagram discussed in section III D.

The magnetization process of SrGd_2O_4 with $H \parallel c$ (the easy axis for this material) is more complicated, with

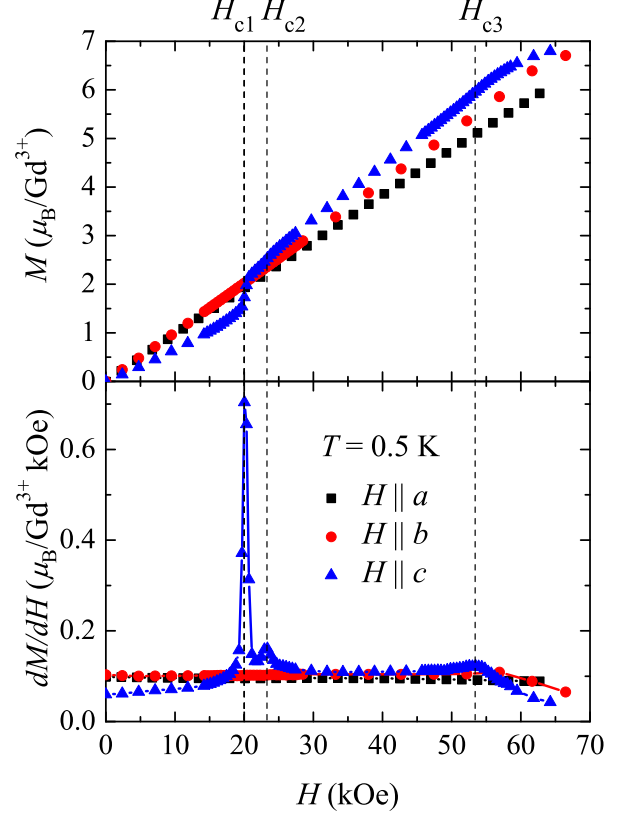


FIG. 5: Top: Magnetization curves obtained with the field applied along the principal axes of SrGd_2O_4 at 0.5 K in the range of 0 to 70 kOe. Bottom: Field derivatives of the magnetization. The field induced transitions are indicated by dashed lines at $H_{c1} = 20.0$ kOe, $H_{c2} = 23.3$ kOe and $H_{c3} = 53.4$ kOe. Between H_{c1} and H_{c2} , when $H \parallel c$, a narrow plateau in dM/dH is observed at approximately one third of the value for the maximum moment along the c axis.

three in-field transitions seen for data collected at 0.5 K. The initial rise in the magnetization is accompanied by a maximum in dM/dH at $H_{c1} \approx 20.0$ kOe, and then for a small region of the applied field the magnetization shows much slower growth (with a minimum in dM/dH seen at ~ 22 kOe), and then another small rise up to a second maximum in dM/dH at $H_{c2} \approx 23.3$ kOe. Thus, it is possible that for SrGd_2O_4 H_{c1} and H_{c2} confine a narrow plateau with an average magnetization value of $2.3 \mu_B$ (which is equal to roughly a third of the saturation magnetization value observed with $H \parallel c$). Such a plateau can be a sign of a field induced stabilization of a collinear *two-spins-up-one-spin-down* (uud) magnetic structure, in which on each triangle of spins, two are pointing up along the field and the third spin pointing down anti-parallel to the field direction. Similar, albeit more distinct, plateaus have been observed in the magnetization curves of the other SrLn_2O_4 compounds,²¹ and thus, the stabilization

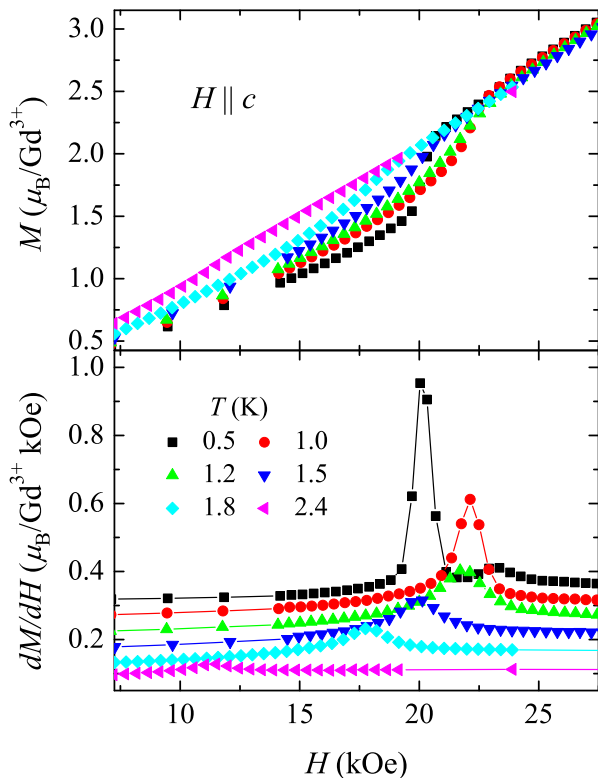


FIG. 6: Top: Magnetization curves for SrGd₂O₄ obtained at several temperatures in the field range of 7.5 to 27.5 kOe, for $H \parallel c$. Bottom: Field derivatives of the magnetization, the curves have been offset by 0.05 units along the vertical axis. The double peak in the derivative of magnetization seen in the data collected at 0.5 K becomes only a single peak at higher temperatures, and this single maximum in dM/dH is initially shifted up, and then down in field as the temperature is increased.

of the uud spin structure could be a common feature of this family of materials. A third field induced transition for $H \parallel c$ is observed at $H_{c3} \approx 53.4$ kOe, and in even higher applied fields the magnetization shows signs of approaching saturation. The demagnetization corrections only have a small impact on the position of the field-induced phase transitions at H_{c1} and H_{c2} (of under 2%), but a somewhat larger effect on the position of H_{c3} (of $\sim 5\%$). These field induced transitions have been confirmed across multiple independently aligned SrGd₂O₄ samples and their positions in field remain robust. Also, no hysteresis with the applied field along any of the principal crystal axes of SrGd₂O₄ is observed, as the magnetization data collected upon increasing and decreasing field coincides.

To further investigate the region of the applied field around H_{c1} and H_{c2} with $H \parallel c$ for SrGd₂O₄, $M(H)$

data was collected at several temperatures, and this and the derivative of the magnetization are shown in Fig. 6. The double peak in the derivative of magnetization seen in the data collected at 0.5 K becomes only a single peak at higher temperatures, and this single maximum in dM/dH is initially shifted up, and then down in field as the temperature is increased. Since the two peaks in dM/dH at H_{c1} and H_{c2} split from a single peak as the temperature is lowered, and with the extra data points obtained for plotting out the phase diagram for $H \parallel c$ (see Section III C), it seems plausible that at even lower temperatures the uud state would govern a larger region of the applied field.

The magnetization processes in all of the SrLn₂O₄ compounds are highly anisotropic. In SrEr₂O₄, the magnetic anisotropy is of pronounced easy-plane type,^{18,21} while in SrHo₂O₄ and SrDy₂O₄ an Ising-type behavior is observed (with different directions of an easy-axis on two different crystallographical sites for the magnetic ions).^{21,24} In SrYb₂O₄, the magnetization measured with $H \parallel c$ is much higher than in perpendicular directions, but the magnetic moments seem to have significant components along all three main symmetry axes.¹⁹ In SrGd₂O₄, which is not affected by crystal field splitting, almost all of the non-trivial magnetic behavior occurs for fields applied along the c axis and it is possible that this direction is an effective easy-axis of magnetization. The fact that low-temperature magnetization below H_{c1} is significantly large (well above $1 \mu_B$ per Gd³⁺) implies that the low-field magnetic structure in SrGd₂O₄ is non-collinear.

An interesting parallel to the behavior of SrGd₂O₄ may be found by looking at the Gd pyrochlore titanate. A Heisenberg-type antiferromagnet, Gd₂Ti₂O₇ orders magnetically at about 1 K.³⁷ Despite the absence of a significant single ion anisotropy for the Gd³⁺ ions, Gd₂Ti₂O₇ shows a highly anisotropic behavior in applied fields at lower temperatures,³⁸ with multiple field-induced transitions.³⁹ In Section III D, we will further extend the analogy between the high-field behavior of SrGd₂O₄ and Gd₂Ti₂O₇, after first discussing the relevant $C(H)/T$ results below.

C. Specific heat

The temperature dependence of the specific heat, $C(T)$, of single crystals of SrGd₂O₄ and of the non-magnetic isostructural compounds SrLu₂O₄ and SrY₂O₄ were measured in zero field. The $C(T)/T$ curves are shown in Fig. 7. Two λ -anomalies which correspond to transitions to long-range magnetic order are observed at $T_{N1} = 2.73$ K and $T_{N2} = 0.48$ K. The lattice contribution to the specific heat of SrGd₂O₄ can be estimated by measuring the heat capacity of two single crystal non-magnetic isostructural compounds: SrY₂O₄ and SrLu₂O₄. At temperatures below ~ 6 K, the lattice contribution to the specific heat of SrGd₂O₄ is negligible

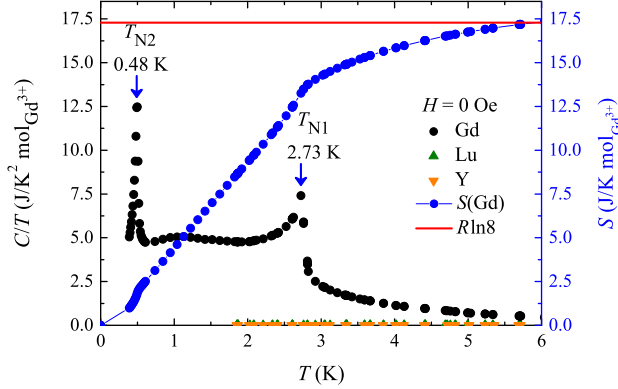


FIG. 7: Temperature dependence of the specific heat divided by temperature of SrGd_2O_4 and of the nonmagnetic isostructural compounds SrLu_2O_4 and SrY_2O_4 measured in zero field. Two λ -anomalies are observed at $T_{N1} = 2.73$ K and $T_{N2} = 0.48$ K. The entropy is calculated as the area under the $C(T)/T$ curve which has been linearly extended to zero at $T = 0$ K, with the scale given on the righthand axis. By 6 K, the full magnetic contribution to the entropy expected for the Gd^{3+} , $J = S = 7/2$, system is recovered, as indicated by the solid line positioned at $R \ln 8$.

compared to the magnetic contribution, and thus the magnetic entropy can be estimated by integrating the $C(T)/T$ curve which has been extended linearly down to $T = 0$ K. It should be noted that, for a powder sample, measurements of the specific heat were also made using a dilution insert for the PPMS which extended the temperature range of the zero field measurements down to 0.05 K (data not shown). These measurements confirmed that below T_{N2} $C(T)/T \rightarrow 0$ in a linear fashion as $T \rightarrow 0$ K, and that no more low-temperature transitions are present in the material down to 0.07 mK. The entropy curve for the single crystal measurements is also shown in Fig. 7, and the (blue) righthand axis should be used for the appropriate scale. It appears that by 6 K the full magnetic entropy expected for the Gd^{3+} , $J = 7/2$, system is recovered.

From magnetic susceptibility and magnetization data it has become apparent that for the fields applied along the a and b axes, SrGd_2O_4 shows no signs of any additional field-induced transitions apart from the transition from an ordered phase into a fully polarized state. With this in mind, the specific heat was measured for the fields applied along the c axis in a broad range of both fields and temperatures. The data for $C(T)/T$ in several applied fields are shown in the top panel of Fig. 8. The two phase transitions in SrGd_2O_4 , whose temperature is defined by the λ anomalies, seen in $H = 0$ Oe move closer together upon increasing the strength of the applied field. The transitions ‘merge’ into a single broad peak seen when $C(T)$ is measured in 22.5 kOe, and after subsequent increases of the field this single peak is first

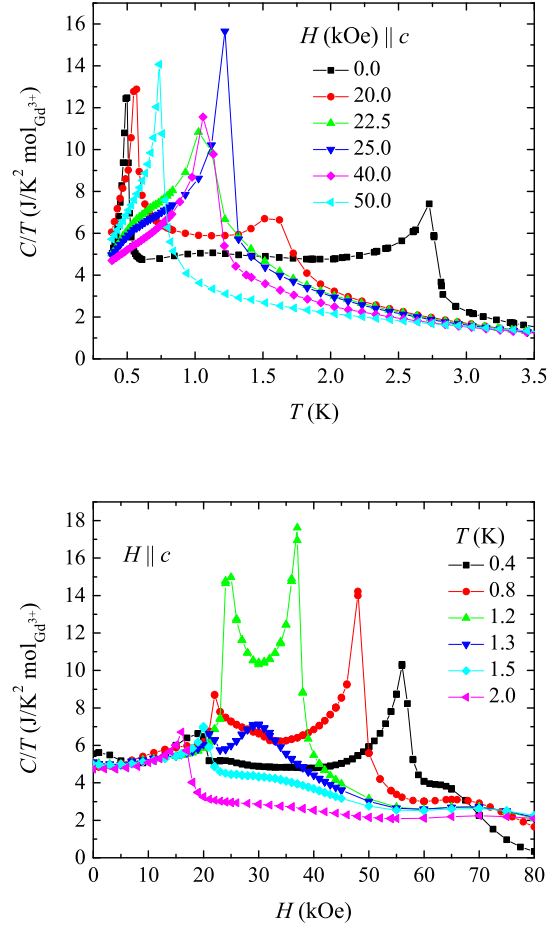


FIG. 8: Top: Temperature dependence of the specific heat divided by temperature of SrGd_2O_4 in several fields for $H \parallel c$. The two peaks associated with the transitions move closer with higher applied fields, before merging and then this single peak is shifted to lower temperatures in the highest applied fields. Bottom: Field dependence of the specific heat divided by temperature at several temperatures for $H \parallel c$. At the lowest temperature, two peaks are observed in $C(H)$. As the temperature is raised, the peaks move closer together and eventually merge. For even higher temperatures, this single peak is suppressed and moves to lower fields.

shifted to higher and then lower temperatures. $C(H)/T$ was also measured for $H \parallel c$, and the data is shown in the bottom panel of Fig. 8. At the lowest measured temperature, two peaks are visible in the heat capacity data. As the temperature is increased, these two peaks move closer together, and in a small temperature range (between 1.2 and 1.3 K) are quickly suppressed in intensity before merging together at temperatures around 1.5 K. Subsequent increases in the temperature just shift this single peak to lower fields. All of the specific heat data collected for $H \parallel c$ are also used to construct the $H \parallel c$ phase diagram for SrGd_2O_4 , which is described below.

The results of heat capacity measurements as a func-

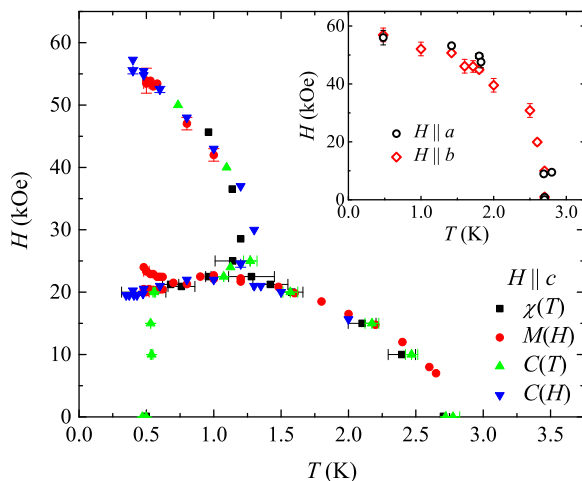


FIG. 9: Main panel: Magnetic H - T phase diagram for SrGd_2O_4 with the field applied along the c axis constructed from the susceptibility, magnetization and specific heat curves. Inset: Field dependence of the upper critical temperature, T_{N1} , as observed in magnetization $M(H)$ and $M(T)$ measurements for $H \parallel a$ and $H \parallel b$. The methods used to obtain the phase boundaries are given in Ref. 41.

tion of both temperature and magnetic field give direct information about the boundaries of the phase transitions observed in SrGd_2O_4 , and these measurements demonstrate that SrGd_2O_4 is very different to other SrLn_2O_4 compounds. For SrGd_2O_4 , magnetic susceptibility and specific heat measurements indicate that at least two transitions take place in zero-field at low temperatures, at 2.73 and 0.48 K, and no other SrLn_2O_4 compound measured so far shows two separate transitions to different long-range orders in zero applied field. Specific heat measurements, on SrDy_2O_4 ,²⁰ SrHo_2O_4 ,⁴⁰ SrEr_2O_4 ,²⁶ and SrYb_2O_4 ¹⁹ indicate the presence of short-range correlations developing at temperatures much higher than the observed transition temperatures in these materials. In the specific heat data collected for SrGd_2O_4 , however, short-range correlations are limited to a small temperature range just above the transition temperature of 2.73 K. In contrast to SrGd_2O_4 , the magnetic entropy contribution recovered at relatively low temperatures in SrEr_2O_4 ,²⁶ SrYb_2O_4 ,¹⁹ and SrDy_2O_4 ²⁰ amounts to $R \ln 2$, while in SrHo_2O_4 it is $R \ln 5$,⁴⁰ although this value is obtained over a much wider temperature range and without subtracting the nuclear Schottky anomaly.

D. H - T phase diagram of SrGd_2O_4

By collating all of the susceptibility, magnetization, and specific heat data for $H \parallel c$, a magnetic field-temperature phase diagram may be constructed for SrGd_2O_4 , and this is shown in main panel of Fig. 9.⁴¹ The phase diagram reveals the rich and complex mag-

netic behavior of SrGd_2O_4 when $H \parallel c$. In addition to the paramagnetic regime, four other phases may be identified by looking at the boundaries on the diagram. This behavior is contrasted with a somewhat simpler response observed on application of magnetic field in directions orthogonal to c . For $H \parallel a$ and $H \parallel b$, the inset to Fig. 9 shows how the upper-temperature transition T_{N1} gradually decreases in increasing fields. In this case, the magnetization measurements (limited to temperatures above 0.5 K) seem to indicate a single transition from a magnetically ordered to a disordered phase. It might be interesting to extend the magnetization measurement to the temperatures below $T_{N2} = 0.48$ K and check how the lowest-temperature phase responds to the application of field along all these crystallographical axes.

For all three directions of an applied field, the value of the upper-field transition H_{c3} extrapolated to zero temperature returns approximately 60 kOe. Treated as a saturation field, this value could potentially be used to estimate the strength of the antiferromagnetic exchange interactions J_{ij} provided that the number of interacting neighbors is known. In the absence of such information and because of the possible competition between different exchange links involved, neither H_{sat} nor the θ_{CW} can be reliably converted to estimate J_{ij} , but what can be stated is that the energy of the exchange interactions in SrGd_2O_4 amounts to just a few kelvin. If this is the case, then it is rather obvious that given the relatively short Gd^{3+} - Gd^{3+} separation (3.48 Å along the c axis) and a large magnetic moment ($J = 7/2$), dipolar interactions, which only for the nearest neighbors amount to roughly a kelvin in units of temperature, cannot simply be disregarded – they must be taken into account as a leading perturbation to a purely exchange Hamiltonian.

In zero field, two transitions take place in SrGd_2O_4 . The magnetic structures of the different phases remain unknown, but at least for the intermediate temperature regime a non-zero susceptibility and magnetization rule out a simple collinear ordering. With the application of field along the c axis of SrGd_2O_4 , at the lowest temperature, three field-induced transitions are observed at H_{c1} , H_{c2} and H_{c3} . It remains to be confirmed that the phase between H_{c1} and H_{c2} corresponds to the order observed in other SrLn_2O_4 compounds.²¹

An interesting observation to make is on the nature of the high-field phase (above H_{c3}) at low temperatures usually labeled as a “fully-polarized state”. The magnetization continues to grow at a significant rate above H_{c3} (see Fig. 5) and the magnetic heat capacity is also far from zero (the bottom panel in Fig. 8 shows that the heat capacity approaches zero only in much stronger fields around 80 kOe). This behavior is reminiscent of what has been observed in another Gd^{3+} containing compound, the pyrochlore titanate. In particular, the field dependence of the heat capacity divided by temperature observed in $\text{Gd}_2\text{Ti}_2\text{O}_7$ (see Fig. 3 in Ref. 38) seems to be remarkably similar to what is shown in Fig. 8 for SrGd_2O_4 . One could argue that such behavior should

be attributed to the influence of dipole-dipole interactions which tilt the magnetic moments away from the field direction even in a nominally fully-polarized state.

The results of the bulk property measurements on SrGd_2O_4 would merit further experimental study using neutron diffraction. However, such experiments are challenging to carry out due to the large absorption cross-section of naturally abundant Gd.⁴² To date, only a few preliminary single crystal neutron diffraction measurements have been performed on SrGd_2O_4 , using the D9 instrument at the Institut Laue-Langevin, Grenoble, France in zero applied field.⁴³ These indicate that the magnetic order that appears below 2.73 K is commensurate with the lattice, and can be indexed with the propagation vector $\mathbf{k} = 0$. Other members of the SrLn_2O_4 family, such as SrEr_2O_4 and SrHo_2O_4 , also develop $\mathbf{k} = 0$ order (or partial order in the case of Ho) involving half of the magnetic Ln ions which occupy the same crystallographical position, while the other half of the Ln ions form a completely different magnetic arrangement.^{22,23,26,28} Thus a $\mathbf{k} = 0$ antiferromagnetic order seems to be a common feature in this family of compounds, but it remains to be seen if the lower-temperature transition found in SrGd_2O_4 at 0.48 K is related to an ordering of the second half of the Gd ions or is it a further readjustment of the $\mathbf{k} = 0$ phase.

IV. CONCLUSIONS

The first high quality single crystals of SrGd_2O_4 have been grown using the floating zone technique, and these have been investigated by the specific heat, magnetization and susceptibility measurements. SrGd_2O_4 orders magnetically at 2.73 K, a temperature lower than the measured Weiss temperatures, $\theta_{\text{CW}} = -10.4(1)$ K, with a further transition taking place at 0.48 K. The data reveal an anisotropic nature of the low-temperature mag-

netic structure, with the c axis found to be the easy axis in the system. At the lowest accessible experimental temperatures, three field induced transitions have been observed in SrGd_2O_4 for $H \parallel c$. It may be conjectured that one of the phases stabilised with the applied field is an up-up-down spin order such as that seen in the other members of the SrLn_2O_4 family. For the magnetic field applied along the c axis, the magnetic phase diagram of SrGd_2O_4 , as a function of field and temperature, was carefully mapped out.

The data illustrate that there is a large difference between the magnetic behavior of SrGd_2O_4 and that of the SrHo_2O_4 , SrEr_2O_4 and SrDy_2O_4 compounds investigated previously, even though the positions of the magnetic ions and the strength of the exchange interactions are similar. This is not totally unexpected as the low-temperature properties of SrGd_2O_4 have to be quite different compared to the other SrLn_2O_4 compounds in which the spin-orbit coupling and crystal field anisotropies play a much more important role. An interesting point for further research is to establish the hierarchy of the magnetic interactions in SrGd_2O_4 , in particular the relationship between the exchange interactions and the dipolar forces and their influence on the selection of the ground state in this frustrated antiferromagnet.

ACKNOWLEDGMENTS

We are grateful to B. Z. Malkin and M. L. Plumer for valuable discussions. The magnetometer used in this research was obtained through the Science City Advanced Materials project: Creating and Characterising Next Generation Advanced Materials, with support from Advantage West Midlands (AWM) and was part funded by the European Regional Development Fund (ERDF). The authors acknowledge financial support from the EP-SRC, U.K. under grant EP/I007210/1.

-
- ¹ A. P. Ramirez, *Annu. Rev. Mater. Sci.* **24**, 453 (1994).
 - ² A. P. Ramirez, *Physics of Magnetism and Magnetic Materials*, vol. 13 (Elsevier, Amsterdam, 2001).
 - ³ H. T. Diep, ed., *Frustrated Spin Systems* (World Scientific, Singapore, 2005).
 - ⁴ A. P. Ramirez, G. P. Espinosa, and A. S. Cooper, *Phys. Rev. Lett.* **64**, 2070 (1990).
 - ⁵ M. F. Collins and O. A. Petrenko, *Can. J. Phys.* **75**, 605 (1997).
 - ⁶ R. Moessner, S. L. Sondhi, and P. Chandra, *Phys. Rev. B* **64**, 144416 (2001).
 - ⁷ P. Schiffer, A. P. Ramirez, D. A. Huse, and A. J. Valentino, *Phys. Rev. Lett.* **73**, 2500 (1994).
 - ⁸ O. Tchernyshyov, *Phys. Rev. Lett.* **93**, 157206 (2004).
 - ⁹ J. S. Gardner, M. J. P. Gingras, and J. E. Greedan, *Rev. Mod. Phys.* **82**, 53 (2010).
 - ¹⁰ J. Villain, *Z. Phys. B* **33**, 31 (1979).
 - ¹¹ K. Binder and A. P. Young, *Rev. Mod. Phys.* **58**, 801 (1986).
 - ¹² R. Moessner and J. T. Chalker, *Phys. Rev. Lett.* **80**, 2929 (1998).
 - ¹³ B. Canals and C. Lacroix, *Phys. Rev. Lett.* **80**, 2933 (1998).
 - ¹⁴ L. M. Lopato and A. E. Kushchevskii, *Ukrainskii Khimicheskii Zhurnal* **39**, 7 (1973).
 - ¹⁵ B. F. Decker and J. S. Kasper, *Acta Cryst.* **10**, 332 (1957).
 - ¹⁶ The Gd^{3+} - Gd^{3+} bond lengths are derived from the refined structural parameters presented in Section II.
 - ¹⁷ H. Karunadasa, Q. Huang, B. G. Ueland, J. W. Lynn, P. Schiffer, K. A. Regan, and R. J. Cava, *Phys. Rev. B* **71**, 144414 (2005).
 - ¹⁸ G. Balakrishnan, T. J. Hayes, O. A. Petrenko, and D. M^cK Paul, *J. Phys.: Condens. Matter* **21**, 012202 (2009).
 - ¹⁹ D. L. Quintero-Castro, B. Lake, M. Reehuis, A. Niazi, H. Ryll, A. T. M. N. Islam, T. Fennell, S. A. J. Kimber,

- B. Klemke, J. Ollivier, et al., Phys. Rev. B **86**, 064203 (2012).
- ²⁰ T. H. Cheffings, M. R. Lees, G. Balakrishnan, and O. A. Petrenko, J. Phys.: Condens. Matter **25**, 256001 (2013).
- ²¹ T. J. Hayes, O. Young, G. Balakrishnan, and O. A. Petrenko, J. Phys. Soc. Japan **84**, 024708 (2012).
- ²² O. Young, L. C. Chapon, and O. A. Petrenko, J. Phys.: Conf. Ser. **391**, 012081 (2012).
- ²³ O. Young, A. R. Wildes, P. Manuel, B. Ouladdiaf, D. D. Khalyavin, G. Balakrishnan, and O. A. Petrenko, Phys. Rev. B **88**, 024411 (2013).
- ²⁴ A. Fennell, V. Y. Pomjakushin, A. Uldry, B. Delley, B. Prévost, A. Désilets-Benoit, A. D. Bianchi, R. I. Bewley, B. R. Hansen, T. Klimczuk, et al., Phys. Rev. B **89**, 224511 (2014).
- ²⁵ J.-J. Wen, W. Tian, V. O. Garlea, S. M. Koohpayeh and T. M. McQueen, H.-F. Li, J.-Q. Yan, D. Vaknin and C. L. Broholm, arXiv:1407.1341.
- ²⁶ O. A. Petrenko, G. Balakrishnan, N. R. Wilson, S. de Brion, E. Suard, and L. C. Chapon, Phys. Rev. B **78**, 184410 (2008).
- ²⁷ O. A. Petrenko, L. C. Chapon, C. Ritter, and T. J. Hayes, ILL Exp. Report 5-31-1695 (2007).
- ²⁸ T. J. Hayes, G. Balakrishnan, P. P. Deen, P. Manuel, L. C. Chapon, and O. A. Petrenko, Phys. Rev. B **84**, 174435 (2011).
- ²⁹ O. A. Petrenko, Low Temperature Physics **40**, 106 (2014).
- ³⁰ Y. Doi, W. Nakamori, and Y. Hinatsu, J. Phys.: Condens. Matter **18**, 333 (2006).
- ³¹ T. Besara, M. S. Lundberg, J. Sun, D. Ramirez, L. Dong, J. B. Whalen, R. Vasquez, F. Herrera, J. R. Allen, M. W. Davidson, et al., Progress in Solid State Chemistry (2014).
- ³² A. A. Aczel, L. Li, V. O. Garlea, J.-Q. Yan, F. Weickert, M. Jaime, B. Maiorov, R. Movshovich, L. Civale, V. Keppens and D. Mandrus, arXiv:1407.4098.
- ³³ A. A. Coelho, *Topas-academic, version 4.1*, <http://www.topas-academic.net> (1992–2007).
- ³⁴ A. Aharoni, J. Appl. Phys. **83**, 3432 (1998).
- ³⁵ N. Shirakawa, H. Horinouchi, and Y. Yoshida, J. Magn. Magn. Mater. **272–276**, e149 (2004).
- ³⁶ C. Kittel, *Introduction to Solid State Physics* (John Wiley and Sons, New York, 1996), 7th ed.
- ³⁷ N. P. Raju, M. Dion, M. J. P. Gingras, T. E. Mason, and J. E. Greedan, Phys. Rev. B **59**, 14489 (1999).
- ³⁸ O. A. Petrenko, M. R. Lees, G. Balakrishnan, and D. McK Paul, Phys. Rev. B **70**, 012402 (2004).
- ³⁹ O. A. Petrenko, M. R. Lees, G. Balakrishnan, V. N. Glazkov, and S. S. Sosin, Phys. Rev. B **85**, 180412(R) (2012).
- ⁴⁰ S. Ghosh, H. D. Zhou, L. Balicas, S. Hill, J. S. Gardner, Y. Qiu, and C. R. Wiebe, J. Phys.: Condens. Matter **23**, 164203 (2011).
- ⁴¹ In order to consistently determine the critical fields and temperatures, when well defined peaks were not observed in $\chi(T)$, dM/dH , $C(T)$ or $C(H)$, (for example, where the transition was observed as a broad peak in susceptibility), the transition point was taken to be at the maximum in $d(\chi T)/dT$. Also, if the transition was observed as a change in the gradient of the measured bulk property (an example for the susceptibility would be the dataset collected in 30 kOe, and for the magnetization measurements this was the method for determining the position of H_{c3}), linear fits to the data were made on either side of the change in the gradient, and the transition point was defined to be where these two lines cross.
- ⁴² V. F. Sears, Neutron News **3**, 26 (1992).
- ⁴³ O. Young, G. Nénert, G. Balakrishnan, and O. A. Petrenko (2013), unpublished.